

A New Fusion Algorithm for Simultaneously Improving Spatio-Temporal Continuity and Quality of Remotely Sensed Soil Moisture Over the Tibetan Plateau

Yaokui Cui , Chao Zeng , Xi Chen , Wenjie Fan, Haijiang Liu, Yuan Liu, Wentao Xiong, Cong Sun, and Zengliang Luo

Abstract—Spatio-temporally continuous and high-quality soil moisture (SM) is very important for assessing changes in the water cycle and climate, especially over the Tibetan plateau (TP). Data fusion is an important method to improve the quality of SM product. However, limited observation overlaps between different satellite SM products, caused by inherent gaps, make it difficult to fuse them to create a continuous and high-quality product. In this study, an SM spatio-temporal continuity and quality simultaneously improving algorithm is proposed. The first step of the approach is obtaining spatio-temporally continuous reference data, including land surface temperature (LST), normalized difference vegetation index (NDVI), Albedo, and digital elevation model (DEM). The second step is training the general regression neural network (GRNN) model with all available essential climate variables (ECV) and Fengyun (FY) SM. The last step is predicting the spatio-temporally continuous and high-quality SM using the trained GRNN derived by the spatio-temporal continuity reference data. An implementation of the algorithm on the TP showed that, compared with the original ECV and FY SM, both the continuity and quality of the fused SM product were largely improved in terms of coverage (72.5%), correlation ($R = 0.809$), root mean square

error ($0.081 \text{ cm}^3 \text{ cm}^{-3}$) and bias ($0.050 \text{ cm}^3 \text{ cm}^{-3}$). The algorithm showed a good performance in obtaining spatio-temporal variation fusion weights over the TP. This spatio-temporally continuous and high-quality SM of the TP will help advance our understanding of global and regional changes in water cycle and climate.

Index Terms—Essential climate variables (ECV), Fengyun (FY), general regression neural network (GRNN), quality, soil moisture (SM), spatio-temporal continuity.

I. INTRODUCTION

SOIL moisture (SM) plays a key role in water-energy exchanges between the land surface and the atmosphere, especially for the earth's third pole of the Tibetan plateau (TP) [1], [2]. The SM is widely used in applications such as weather and climate forecasting, droughts and wildfires monitoring, and floods and landslides early warning [3]–[8]. As an easy, direct and convenient large scale method for monitoring SM, satellite remote sensing has received great attention from the applications community in the last decades. Various active-based, passive-based, and merged SM products have been published, such as the Advanced Scatterometer (ASCAT) [9], advance microwave scanning radiometer 2 (AMSR2), soil moisture active passive (SMAP) [2], European space agency (ESA) essential climate variables (ECV) [9], and Fengyun-3B (FY-3B) [10]. There are two main disadvantages in applying these SM products. The first disadvantage is spatio-temporal discontinuity, with gaps caused by low temporal resolution and other algorithm retrieval failures [11], [12]. Second is low quality, including the low variation capturing ability (in correlation coefficient, R) and low accuracy [in root mean square error (RMSE)], which are very important to land surface model assimilations and flood forecasting, respectively [13]. For example, the R and RMSE of different SM products can range from 0.194 to 0.704 and from $0.077 \text{ mm } d^{-1}$ to $0.296 \text{ mm } d^{-1}$ for Maqu sites over TP, respectively [14].

Spatio-temporal continuity is a common requirement of different applications [13]. However, the quality requirements differ across fields. For example, land surface models need an SM product with high variation capturing ability (high R) benefiting from its data assimilation system, while flash-flood predictions

Manuscript received July 2, 2020; revised September 8, 2020, October 1, 2020, November 10, 2020, and November 25, 2020; accepted November 29, 2020. Date of publication December 8, 2020; date of current version January 6, 2021. This work was supported in part by the National Natural Science Foundation of China under Grant 41901348, in part by the Key R&D Program of the Ministry of Science and Technology, China, under Grant 2018YFC1506500, in part by the Strategic Priority Research Program of the Chinese Academy of Sciences under Grant XDA19030203, and in part by the National Key Research and Development Program of China under Grant 2016YFC0500205. (Corresponding authors: Yaokui Cui; Haijiang Liu.)

Yaokui Cui and Wenjie Fan are with the Institute of RS and GIS, School of Earth and Space Sciences, Peking University, Beijing 100871, China, and also with the Beijing Key Laboratory of Spatial Information Integration and Its Applications, Beijing 100871, China (e-mail: yaokuicui@pku.edu.cn; fanwj@pku.edu.cn).

Chao Zeng is with the School of Resource and Environment Science, Wuhan University, Wuhan 430072, China (e-mail: zengchaozc@hotmail.com).

Xi Chen is with the Aerospace Information Research Institute, Chinese Academy of Science, Beijing 100094, China (e-mail: chenxi928@pku.edu.cn).

Haijiang Liu and Cong Sun are with the China National Environmental Monitoring Center, Beijing 100012, China (e-mail: liuhj@cnemc.cn; suncong@cnemc.cn).

Yuan Liu is with China Fire and Rescue Institute, Beijing 102202, China (e-mail: 2008.liuyuan.2008@163.com).

Wentao Xiong and Zengliang Luo are with the Institute of RS and GIS, School of Earth and Space Sciences, Peking University, Beijing 100871, China (e-mail: wtxiong@pku.edu.cn; zengliangluo@pku.edu.cn).

Digital Object Identifier 10.1109/JSTARS.2020.3043336

need a SM product with a good accuracy (low RMSE and bias) because floods typically occur when precipitation exceeds the soil absorption capacity [13], and a SM product that satisfies this requirement is still a long way in the making. Several previous studies have tried to solve these key issues. Cui *et al.* [10] proposed a machine learning and reference data-based reconstruction method to improve the spatio-temporal continuity. However, the SM reconstructed process cannot improve the quality of the original SM product. And a cumulative distribution function (CDF) matching-based fusion algorithm [15] was also proposed trying to further improve the quality of SM product. However, it is difficult to obtain the fusion weight, especially there are only two products. In other previous studies, data fusion methods [1], [16], [17], such as the triple collation method [12], are widely accepted for improving SM quality. The machine learning method also be widely used in data fusion. For example, Van der Schalie *et al.* [18] used a global neural network (NN) approach, with AMSR-E brightness temperature observations from several frequencies as input and the SMOS Level 3 SM product as a reference dataset to train in the common ASMSR-E and SMOS period and applied it to the whole AMSR-E data record from 2003 to 2010. However, the narrow overlap between different satellite SM products/observation limits their fusion and also cannot obtain spatio-temporally continuous SM. Hence, it is necessary to improve simultaneously both the spatio-temporal continuity and quality of SM products, which has received limited attention until now.

In this study, we focus on simultaneously improving spatio-temporal continuity and quality of SM over the TP. To achieve this objective, we: (1) validated the ECV and FY SM products against *in situ* measurements to evaluate whether they were suitable to be fused together; (2) proposed a new SM spatio-temporal continuity and quality simultaneously improving algorithm; (3) and analyzed the new algorithm. This algorithm should be valuable in providing more reliable and effective information on SM for hydrological and climate studies.

II. MATERIALS

A. Study Area

Well known as the third pole and the Asia tower, the TP (25° – 40° N, 70° – 105° E) was selected as the study area (see Fig. 1) [19]. This study area is covered mainly by grassland in the center and eastern parts, bare soil and sparse vegetation in the western and northern portions, and a few forests in the eastern and southern borders. Soil freezes and thaws frequently, especially in the central and western parts. The complex terrain, uneven distribution of water and energy, and a changeable climate cause frequent gaps in the common SM products [10], which limit global change-related studies.

B. In Situ SM Measurements

In this study, two *in situ* measurement networks over the TP (see Fig. 1 and Table I) were used to validate the algorithm. The Maqu network is located in north-eastern part of the TP in a cold humid climate [20]. The network covers an area of approximately 40×80 km having 20 sites located on grasslands. Due

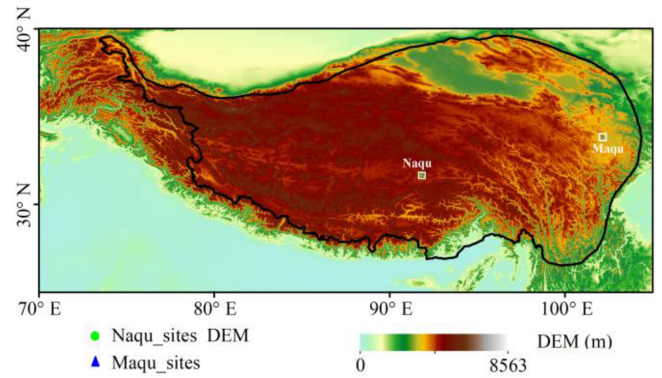


Fig. 1. Study area and location of the both networks on the DEM map, where green and blue symbols represent the distribution of sites in Maqu and Naqu networks, respectively.

TABLE I
MAIN CHARACTERISTICS OF THE MAQU AND NAQU NETWORKS

Networks	Sites	Climate	Depth	Land cover	Date period
Maqu	3	Cold humid	5 cm	Grassland	2012-2014
Naqu	14	Cold semiarid	5 cm	Grassland	2012-2014

TABLE II
DATASETS USED IN THIS STUDY FOR THE PERIOD 2012–2014

Source	Dataset	Variable	Spatio-temporal resolution
MODIS	MOD11C1	LST	0.05°/daily
	MCD43C3	Albedo	0.05°/daily
	MOD13C1	NDVI	0.05°/16-day
ESA	ECV V04.7	SM	0.25°/daily
	FY-3B	SM	0.25°/daily
SRTM	SRTM 90m	DEM	90 m

to the severe local conditions, several sites have discontinued observations. In this study, daily averaged SM measured in the top 5 cm of three sites from 2012 to 2014 within an area of $0.25 \times 0.25^{\circ}$ was used. The multiscale Naqu network is located in the central TP under cold semiarid climate [21]. The Naqu network, covered by grassland, has 56 sites and was set up gradually from 2010. In this study, daily averaged SM measured in the top 5 cm of 14 sites from 2012 to 2014 within an area of $0.25 \times 0.25^{\circ}$ was used. For more details about the Maqu and Naqu networks, readers are kindly referred to Su *et al.* [20] and Yang *et al.* [21], respectively.

C. Satellite Data

The satellite data used in this study are summarized and listed in Table II.

The combined microwave SM ECV product from the European space agency climate change Initiative project version V04.7 (ECV SM V04.7) for the period 2012–2014 was used in this study [11]. This product was generated by merging active SM, including ASCAT and AMI, and passive SM, including

SMOS, SMMR, TMI, SM/I, AMSR-E, and WindSat, observations spanning the years 1978–2019 [11], [22].

The ascending (13:40 local solar time) FY SM from the China Meteorological Administration was also used in this study [15]. This dataset was a retrieval product from the X-band observation by the Microwave Radiation Imager on the FY-3B satellite. The spatial resolution of the original FY SM is 25 km with EASE-Grid projection and was converted to 0.25° to match the ECV SM. It should be noted that the FY-3B SM was not merged into the ECV SM product.

Auxiliary data included moderate-resolution imaging spectroradiometer in version 6 of daily land surface temperature (LST, MOD11C1, 0.05°), daily Albedo (MCD43C3, 0.05°), and 16-day normalized difference vegetation index (NDVI, MOD13C1, 0.05°) were downloaded.¹ The gaps in LST, NDVI, and Albedo were filled using the methods described in Section III-B. The gap-filled LST, NDVI, and Albedo were aggregated from 0.05° to 0.25° spatial resolution. The NDVI was resampled from 16-day to daily using a linear interpolation method.

Due to topographic effects of the LST, we used the SRTM digital elevation model (DEM) with 90 m resolution to reduce it.² The DEM was resampled and reprojected from 90 m to 0.25° using a moving average algorithm.

III. METHODS

The main objective of this study is to simultaneously improve both the spatio-temporal continuity and quality of SM based on two different products. In the soil unfrozen period, remotely sensed land surface variables such as LST, NDVI, and surface albedo can reflect SM changes, due to their controlling effect of SM on surface energy exchange and the ability to reflect vegetation status [23]–[26]. In regional scale, the LST always has terrain effect which can be described by the DEM. NNs can be used to extract information from various input variables. In this study, the general regression neural network (GRNN) was used to extract synergistic information from the original ECV and FY SM based on the land surface variables (reference data). Due to the unreliable relationship between SM and these variables over soil frozen period, the algorithm was only applied during the soil unfrozen period, where the land is not covered by snow (Albedo less than 0.3) and the LST is higher than 0°C . The fusion weights were obtained by the overall performance of the original SM against the land surface variables. This also provided a reference when there is no original SM or only one original SM available. The core of this method is that the weight is decided by the relationship between the original SM and the reference data, and this represents a big difference from ground data-based fusion methods [27].

A. GRNN to Improve SM Product

The GRNN model is a kind of radial basis function NN, transforming the data from a low to a high-dimensional space [28]. It has following four layers: input layer, hidden layer, summation

TABLE III
LIST OF METHODS USED IN GENERATING SPATIO-TEMPORALLY CONTINUOUS REFERENCE DATA

Variables	Methods	reference
LST	Multi-temporal Regression	Zeng et al. [31]
NDVI	Harmonic Analysis of Time Series	Zhou et al. [32]
Albedo	Statistics-based Temporal Filter Algorithm	Liu et al. [33]

layer, and output layer. Due to the lack of iterative training, the GRNN can achieve a high learning speed. Meanwhile, it also shows a strong nonlinear mapping ability with a high degree of fault tolerance and robustness, and can work well with a small number of samples. In our previous studies, the GRNN model has been used to improve the SM spatio-temporal resolution with the satisfactory performance [29]. The core idea of the GRNN model is to establish the nonlinear function between input variables (here reference data) and output SM.

$$SM = GRNN(RD) \quad (1)$$

where RD is spatio-temporal continuous reference data, including LST, NDVI, Albedo, and DEM. More details about GRNN can be found in Specht [28].

The performance of GRNN might be sensitive to the training dataset. Hence, the widely used K -fold cross-validation (K -CV) method was adopted to obtain the optimization model [8]. In the K -CV, the training dataset was divided into K subsets and then $K-1$ subsets were selected to optimize the model and 1 remaining subset was used to evaluate it.

B. Generating Spatio-Temporal Continuous Reference Data

To fuse SM products with limited overlap, we used spatio-temporal continuous reference data to bridge the gaps among different SM products. There were four input variables in the reference data; three input variables (LST, Albedo, NDVI) needed to be firstly reconstructed due to cloud contamination. In previous studies, these three variables have been well reconstructed based on the published methods listed in Table III [10], [15], [30]. Reference data were then reprojected and resampled to 0.25° .

C. Spatio-Temporal Continuity and Quality Improving Procedure

The procedure for improving SM spatio-temporal continuity and quality based on the GRNN model is shown in Fig. 2. The first step is data preprocessing, which uses methods mentioned in Section III-B for obtaining spatio-temporal continuous LST (0.25° , daily), Albedo (0.25° , daily), NDVI (0.25° , daily), and DEM (0.25°).

The second step is GRNN model training. The key points in this step are as follows.

- 1) Only the unfrozen period, defined here as $LST > 0^\circ\text{C}$ and Albedo < 0.3 , is considered.
- 2) A moving window with a size of $1^\circ \times 1^\circ$ and year by year is used to improve the model performance.

¹[Online]. Available: <https://search.earthdata.nasa.gov/>

²[Online]. Available: <http://srtm.csi.cgiar.org/>

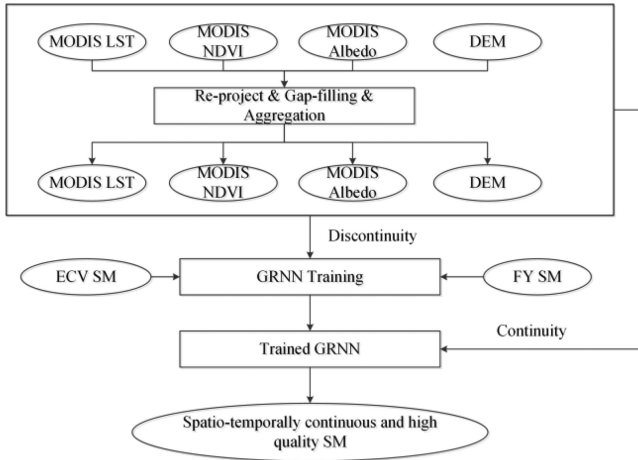


Fig. 2. Flowchart of spatio-temporally continuous SM and quality improving algorithm.

- 3) A union dataset of valid ECV and FY is used as the output layer.
- 4) The entire data is randomly separated into five subsets (four for training and one for testing).
- 5) Running five times with different GRNN models and the GRNN having highest R of testing dataset is selected as the optimization model, due to it is more important to reproduce the relative dynamics of SM rather than their absolute values [22], [34].

Note that the same reference data might be used twice when both ECV and FY have a valid value. The GRNN learns the common features from the union dataset.

The last step is generating spatio-temporally continuous and high-quality SM using the trained GRNN model with spatio-temporal continuous reference data.

D. Input Variable Importance Analysis

It is essential to display the importance of the input variables to further understand the spatio-temporally continuous SM and quality improving algorithm. Here, we propose a normalized root mean square error index (NRMSEI) to describe the relative importance of the input variables

$$\text{NRMSEI} = \frac{\text{RMSE}_i}{\sum_{i=1}^n \text{RMSE}_i} \quad (2)$$

where RMSE_i is the RMSE of model prediction when i th variable is not included against all variables are included, n is the number of input variables.

IV. RESULTS

Given the strong relationship between the reference data and the original ECV (ECV_Ori) and FY (FY_Ori) SM, the GRNN model was applied to generate spatio-temporally continuous and high-quality SM data. In this section, we will analyze the results of each network over the TP, respectively. First, the ECV_Ori and FY_Ori SM were evaluated to show the potential value of fusing them. Second, the fused SM was compared with the

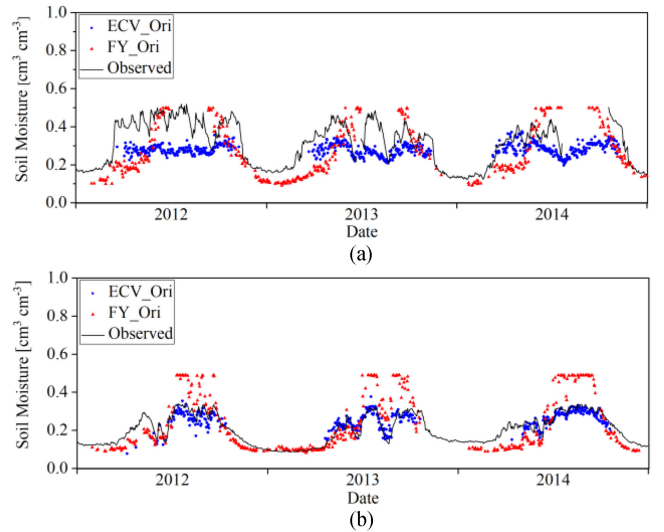


Fig. 3. Time series of the original ECV (ECV_Ori) and FY (FY_Ori) SM against *in situ* observations in the: (a) Maqu and (b) Naqu networks.

original SM to show the improved coverage. Third, the fused SM was compared with the reconstructed ECV (ECV_Rec) and FY (FY_Rec) SM, which are also spatio-temporally continuous, to show the improved quality. At last, the fusion weight and input variable importance were displayed to show more information about this algorithm.

A. Comparison of Original SM Against In Situ Measurements

We evaluated the performance of the ECV_Ori and FY_Ori SM over the TP before the SM spatio-temporal continuity and quality simultaneously improving process. As shown in Fig. 3, the FY_Ori SM has a more uniform distribution than the ECV_Ori SM, although it has less coverage in the middle of the year. This is because the ascending FY overpasses at 13:30 local solar time, while the ECV_Ori has nighttime observations from 0:00 A.M. to 9:30 A.M. where the LST is lower than 13:30 making the ECV_Ori has larger data gaps during winter. Except for the data missing at the start and at the end of the year, FY_Ori SM seems better than ECV_Ori SM in the Maqu network region, with higher R , lower Bias and comparable RMSE (see Table IV). However, in the Naqu network, the ECV_Ori SM performs better than FY_Ori SM with lower RMSE and Bias values as well as higher R value (see Table IV). Compared with previous research works, we found that ECV SM V04.7 differs slightly from its previous version, V04.4, with a decrease in the number of observations but an improvement in the quality, except for the lower R in the Maqu network [15]. The difference between these two products is mainly in the rescaling process, suggesting that the CDF matching has a temporal variation, which will result in unexpected uncertainty in the combined SM product [11], [22]. Overall, the quality of both original ECV and FY SM gave a good foundation for the SM spatio-temporal continuity and quality simultaneously improving process.

TABLE IV
ERROR METRICS OF SM FOR THE MAQU AND NAQU NETWORKS FOR FUSED,
RECONSTRUCTED ECV, AND FY SM

Metric	Maqu			Naqu		
	Fused	ECV_Rec	FY_Rec	Fused	ECV_Rec	FY_Rec
R	0.758	0.492	0.644	0.860	0.801	0.841
RMSE	0.111	0.166	0.117	0.051	0.048	0.093
Bias	0.088	-0.135	-0.041	0.011	-0.013	0.020
N	945	945	945	976	976	976

R is the correlation coefficient, RMSE is the root mean square error, bias is mean bias, and N is the number of samples. Bold numbers represents the best result. RMSE and Bias are both in $\text{cm}^3 \text{cm}^{-3}$.

B. Comparison of Fused SM Against Original SM

Compared with the ECV_Ori and FY_Ori SM, the coverage of fused SM was greatly improved. For the entire TP, the coverage of fused SM (SM_Fused) was improved from 25.5% of ECV_Ori SM and 23.7% of FY_Ori SM to 72.5% of SM_Fused (see Fig. 4). In the Maqu network, the coverage was also significantly improved with the number of points increasing from 664 for ECV_Ori SM and 391 for FY_Ori SM to 945 for SM_Fused. In the Naqu network, while, the coverage was also significantly improved with the number of points increasing from 410 for ECV_Ori SM and 452 for FY_Ori SM to 976 for SM_Fused. Indicating that the coverage was greatly improved against the original ECV and FY SM, while has strong spatio-temporal coverage variation.

Fig. 5(a) and (b) show the spatial pattern of correlation (R) between fused SM and ECV_Ori and FY_Ori SM products over the TP, indicating a high consistency between them. In the most of the study area, R was larger than 0.8 [see Fig. 5(c) and (d)], indicating the strong contribution of the original SM to the variation capturing ability of SM_Fused. The spatial pattern also showed that at least one product has a high contribution (larger than 0.8) to fused SM in terms of variation capturing ability. Additionally, the fused SM has a higher correlation with ECV_Ori SM than with FY_Ori SM in the western TP, but lower in the eastern TP [see Fig. 5(a) and (b)]. The results suggested that the GRNN model had a strong spatial adaptability in extracting information from the original ECV and FY SM.

Fig. 5(e) and (f) show the spatial pattern of RMSE between fused SM and original ECV and FY SM products, indicating a high impact of the original SM on the fused SM. In most parts, the RMSE for the ECV_Ori and FY_Ori SM products is less than $0.05 \text{ cm}^3 \text{cm}^{-3}$ [see Fig. 5(g) and (h)], indicating that the original SM has a strong impact on the accuracy of fused SM. In the middle TP, the ECV_Ori and FY_Ori SM had a comparable impact on the improvements in accuracy of fused SM. However, ECV_Ori SM had a greater impact than FY_Ori SM in the eastern TP, and smallest in the West.

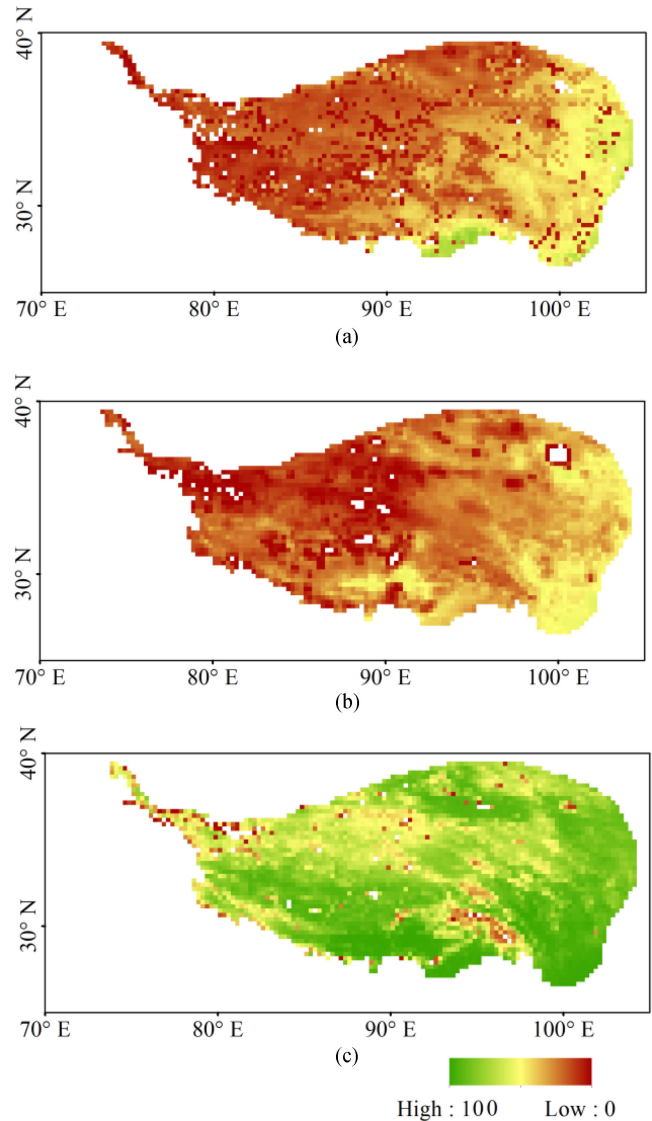


Fig. 4. Temporal coverage for: (a) original ECV SM; (b) original FY SM; (c) fused SM.

C. Comparison of Fused SM Against Reconstructed SM

Compared with the reconstructed ECV and FY SM, the quality of fused SM was also greatly improved (see Fig. 6 and Table IV). In the Maqu network, it can be clearly seen that ECV_Rec SM underestimated SM and FY_Rec SM had a dispersed distribution, indicating that fused SM is more consistent against *in situ* measurements [see Fig. 6(a)]. The R of fused SM was greatly improved compared with ECV_Rec and FY_Rec SM, indicating that the variation capturing ability was significantly improved. The RMSE also was improved compared with ECV_Rec and FY_Rec SM, indicating an improved accuracy. The bias of fused SM ($-0.088 \text{ cm}^3 \text{cm}^{-3}$) was a compromise between ECV_Rec SM ($-0.135 \text{ cm}^3 \text{cm}^{-3}$) and FY_Rec ($-0.041 \text{ cm}^3 \text{cm}^{-3}$), suggesting that there is still room for improvement in this accuracy index. In the Naqu network, fused SM was much closer to the 1:1 line than the reconstructed

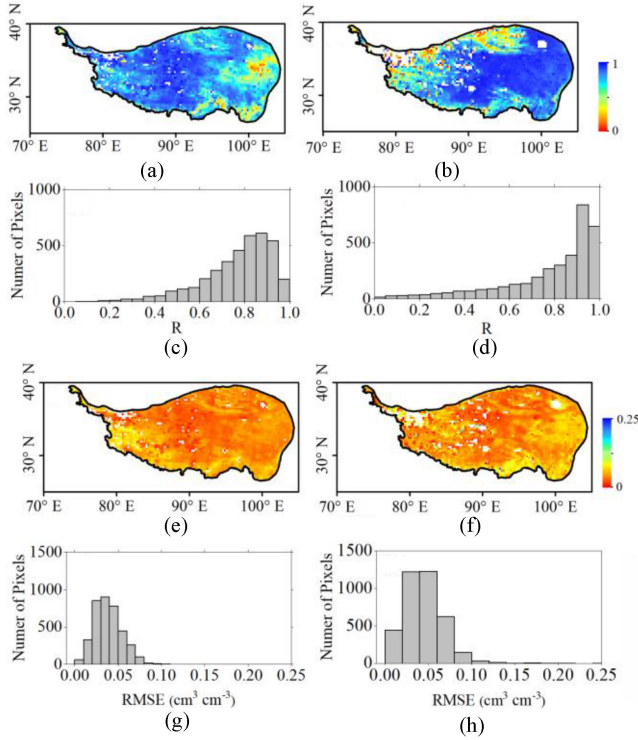


Fig. 5. Correlation (R) and RMSE between fused SM and original SM. (a) and (b) Spatial distribution of R between fused SM and ECV_Ori and FY_Ori SM, respectively. (c) and (d) histogram of R between fused SM and ECV_Ori and FY_Ori SM, respectively. (e) and (f) Spatial pattern of RMSE between SM_fused and ECV_Ori and FY_Ori SM, respectively. (g) and (h) Histogram of RMSE between fused SM and ECV_Ori and FY_Ori SM, respectively.

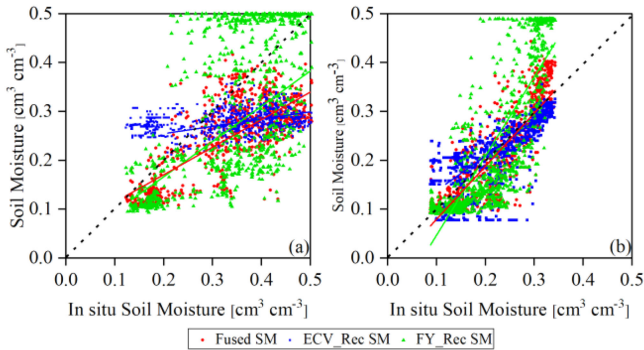


Fig. 6. Scatterplot of fused, reconstructed ECV, and FY SM against *in situ* measurements in the: (a) Maqu network. (b) Naqu network.

SM [see Fig. 6(b)]. Coverage, R and bias were all improved, indicating that fused SM had high spatio-temporal coverage and quality, and only the RMSE was a compromise. Considering that fused SM was obtained from the comprehensive information of reconstructed ECV and FY SM products, the GRNN showed a stronger feature extracting ability and can be applied in SM fusion. It is can also be concluded that the reference data shows acceptable performance in the spatio-temporal continuity and quality simultaneously improving algorithm.

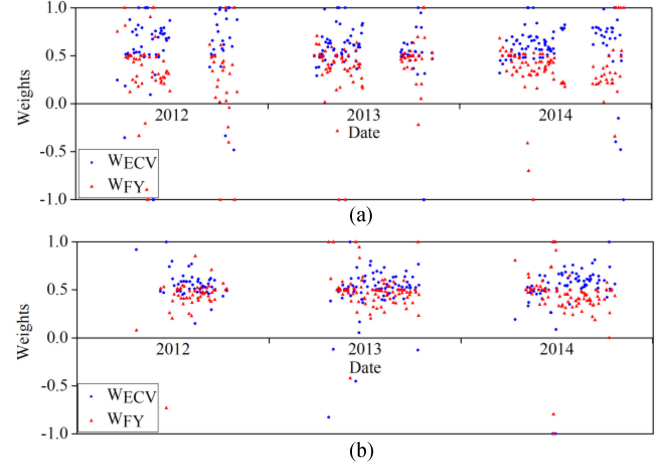


Fig. 7. Time series of weights of original ECV and FY SM in the: (a) Maqu network and (b) Naqu network. Where the weights were larger than 1 or less than -1 , they were set to 1 and -1 , respectively.

V. DISCUSSIONS

A. Fusion Weights Analysis

As a fusion method, it is important to analyze the weights of ECV_Ori and FY_Ori SM to further understand the spatio-temporal continuity and quality simultaneously improving algorithm. The weights could be calculated as

$$W_{ECV} = (SM_{Fused} - SM_{FY}) / (SM_{ECV} - SM_{FY}) \quad (3)$$

$$W_{FY} = 1 - W_{ECV} \quad (4)$$

where W_{ECV} and W_{FY} are the weights of ECV_Ori and FY_Ori SM, respectively. SM_{Fused} , SM_{ECV} , and SM_{FY} are the fused SM, original ECV, and FY SM, respectively. Obviously, the weights can be analyzed only if both the original ECV and FY SM have a valid value.

Fig. 7 shows the time series of W_{ECV} and W_{FY} in the Maqu and Naqu networks, respectively, where the weights larger than 1 or less than -1 were set to 1 and -1 , respectively. The weights showed strong temporal variation in both networks. This was very different from the other fusion methods, such as the TC method, for which it was difficult to obtain temporal variation weights [1], [12]. In most cases, W_{ECV} was larger than W_{FY} at both networks, indicating that ECV_Ori SM contributed more than FY_Ori SM. The reason for this was that the ECV_Ori SM was more consistent with the reference data than FY_Ori SM. On the other hand, the weights were not always located in the range $[0, 1]$ and were less than 0 or larger than 1 in several cases, indicating that the algorithm had a strong adaptive ability. One extremely large W_{FY} of (777.21) was also observed where fused SM was very close to FY_Ori SM.

Fig. 8 shows the spatial pattern of W_{ECV} and W_{FY} in the study area, where only the weights located in the range $[0, 1]$ were included. It clearly can be seen that the weights have a strong spatial variation. This was also the ideal goal for most

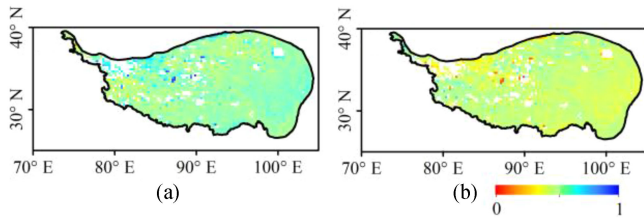


Fig. 8. Spatial distribution of the weights of the original ECV and FY SM during 2012–2014. Where only the mean of weights located in [0], [1] was included.

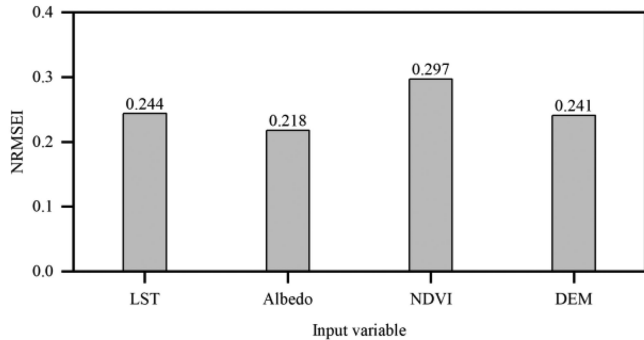


Fig. 9. NRMSEI of input variables in the reference data for the spatio-temporal continuity and quality improving algorithm.

fusion methods [1], [12]. The W_{ECV} is normally larger than W_{FY} , especially in the eastern TP, indicating that the ECV_Ori SM has a greater contribution to the fused SM than FY_Ori SM. It also can be seen that W_{ECV} is significantly larger than W_{FY} in the surrounding of the lakes (most of the blank areas), indicating a more stable performance of ECV SM than FY in these areas.

B. Input Variables Importance Analysis

To analyze the importance of the input variables in the reference data, the NRMSEI was calculated using (2) and the results are shown in Fig. 9. As expected, the NDVI, as an index that represents the SM state at medium- to long-term scales, which supports vegetation growth, was the most important variable (NRMSEI = 0.297). As a widely accepted point, LST, which represents the SM state at short-term scales and is widely used in SM retrieval algorithms, was the second most important variable (NRMSEI = 0.244) [23]. However, the static reference data of DEM also played an important role, due to the LST has a strong terrain effect. The Albedo became the last most important variable, which has the strong negative relationship with SM.

C. Advantages and Limitations of This Study

With the help of the gap-filled reference data, the GRNN model in this study was successfully used to simultaneously improve spatio-temporal continuity and quality of remotely sensed SM over the TP. Although the gap-filling algorithm can improve the spatio-temporal continuity of remotely sensed SM (e.g., [10]), the quality of the gap-filled SM was limited by the quality of the original SM products, which have large uncertainty showed by the validation against *in situ* measurements

due to retrieval algorithm or the related input parameters [14], [35]. Hence, it is necessary to fuse different remotely sensed SM products. Compared with the weight analysis-based fusion algorithm (e.g., [1]), the proposed fusion algorithm is easier to obtain the fusion weight with spatio-temporal variation to enhance the quality of SM. And, fused SM can much better reflect temporal variability and accuracy in SM. The developed SM fusion algorithm in this study would help enhance the applications of SM in climate change over the TP and also for the global. In this study, the fusion algorithm was only evaluated over the TP for ECV and FY SM. Future studies using the fusion algorithm or on other remotely sensed SM products under a wider range of environmental conditions will be performed to further evaluate it.

VI. CONCLUSION

The main objective of this study was to propose a new fusion algorithm for simultaneously improving SM spatio-temporal continuity and quality over the TP. The new algorithm has the following two features: 1) it enhances quality of SM in the variation capturing ability and accuracy; 2) it significantly improves the SM coverage. In this study, based on the GRNN model, the information contained in the ECV and FY SM products was extracted by integrating land surface parameters (e.g., LST, Albedo, and NDVI) and auxiliary parameters (e.g., DEM). The following four main conclusions were derived from this study.

- 1) The complementary and quality of both original ECV and FY SM laid a good foundation for the implementation of the fusion.
- 2) The overall spatio-temporal continuity and quality of the fused SM is higher than the original SM products.
- 3) The GRNN model can obtain spatio-temporal variation weights And, in this study, ECV SM contributed more than FY SM to SM_Fused.
- 4) NDVI played the most important role in the whole process, and LST and Albedo were also very important.

In the future, developing high quality and spatio-temporally continuous SM at hydrological scales (e.g., 1 km) and field scales (e.g., 30 m) will be discussed.

ACKNOWLEDGMENT

The authors would like to thank K. Yang for providing the *in situ* data. They also would like to thank the National Satellite Meteorological Center of China (<http://data.nsmc.org.cn>), European Space Agency (<https://esa-soilmoisture-cci.org>) and National Aeronautics and Space Administration (<https://www.nasa.gov>), for the provision of FY, ECV, and MODIS products.

REFERENCES

- [1] W. Wagner, W. Dorigo, R. D. Jeu, D. Fernandez, and M. Ertl, "Fusion of active and passive microwave observations to create an essential climate variable data record for soil moisture," *ISPRS Ann. Photogrammetry, Remote Sens. Spatial Inf. Sci.*, pp. 315–321, vol. I-7, 2012.
- [2] D. Entekhabi *et al.*, "The soil moisture active passive (SMAP) mission," *Proc. IEEE*, vol. 98, no. 5, pp. 704–716, May 2010.
- [3] J. Blunden *et al.*, "State of the climate in 2015," *Bull. Amer. Meteorological Soc.*, vol. 97, no. 8, pp. Si–S275, 2016.

- [4] M. Rodell *et al.*, "The observed state of the water cycle in the early twenty-first century," *J. Climate*, vol. 28, no. 21, pp. 8289–8318, 2015.
- [5] N. Nicolai-Shaw, L. Gudmundsson, M. Hirschi, and S. Seneviratne, "Long-term predictability of soil moisture dynamics at the global scale: Persistence versus large-scale drivers," *Geophys. Res. Lett.*, vol. 43, pp. 8554–8562, 2016.
- [6] H. Carrão, S. Russo, G. Sepulcre-Canto, and P. Barbosa, "An empirical standardized soil moisture index for agricultural drought assessment from remotely sensed data," *Int. J. Appl. Earth Obs.*, vol. 48, pp. 74–84, Jun. 1, 2016.
- [7] F. Wen, W. Zhao, Q. Wang, and N. Sánchez, "A value-consistent method for downscaling SMAP passive soil moisture with MODIS products using self-adaptive window," *IEEE Trans. Geosci. Remote*, vol. 58, no. 2, pp. 913–924, Feb. 2020.
- [8] W. Zhao, N. Sánchez, H. Lu, and A. Li, "A spatial downscaling approach for the SMAP passive surface soil moisture product using random forest regression," *J. Hydrol.*, vol. 563, pp. 1009–1024, Aug. 1, 2018.
- [9] W. Wagner *et al.*, "The ASCAT soil moisture product: A review of its specifications, validation results, and emerging applications," (in English), *Meteorologische Zeitschrift*, vol. 22, no. 1, pp. 5–33, Feb. 2013. [Online]. Available: <Go to ISI>://WOS:000318226200002
- [10] Y. Cui *et al.*, "Validation and reconstruction of FY-3B/MWRI soil moisture using an artificial neural network based on reconstructed MODIS optical products over the Tibetan plateau," *J. Hydrol.*, vol. 543, pp. 242–254, 2016.
- [11] W. Dorigo *et al.*, "ESA CCI soil moisture for improved earth system understanding: State-of-the art and future directions," *Remote Sens. Environ.*, vol. 203, pp. 185–215, Dec. 15, 2017.
- [12] A. Gruber, W. A. Dorigo, W. Crow, and W. Wagner, "Triple collocation-based merging of satellite soil moisture retrievals," *IEEE Trans. Geosci. Remote Sens.*, vol. 55, no. 12, pp. 6780–6792, Dec. 2017.
- [13] D. Entekhabi, R. H. Reichle, R. D. Koster, and W. T. Crow, "Performance metrics for soil moisture retrievals and application requirements," *J. Hydrometeorol.*, vol. 11, no. 3, pp. 832–840, 2010.
- [14] J. Zeng, Z. Li, Q. Chen, H. Bi, J. Qiu, and P. Zou, "Evaluation of remotely sensed and reanalysis soil moisture products over the Tibetan plateau using in-situ observations," *Remote Sens. Environ.*, vol. 163, pp. 91–110, Jun. 16, 2015.
- [15] Y. Cui *et al.*, "A two-step fusion framework for quality improvement of a remotely sensed soil moisture product: A case study for the ECV product over the Tibetan plateau," *J. Hydrol.*, vol. 587, Aug. 1, 2020, Art. no. 124993.
- [16] C. Montzka *et al.*, "Active and passive L-band microwave remote sensing for soil moisture - A test-bed for SMAP fusion algorithms," *IEEE Conf. Geoscience and Remote Sensing Symposium*, pp. 2427–2430, 2014.
- [17] H. Jiang, H. Shen, X. Li, C. Zeng, and F. Lei, "Extending the SMAP 9-km soil moisture product using a spatio-temporal fusion model," *Remote Sens. Environ.*, vol. 231, 2019, Art. no. 111224.
- [18] R. Van der Schalie *et al.*, "The effect of three different data fusion approaches on the quality of soil moisture retrievals from multiple passive microwave sensors," *Remote Sens. Basel*, vol. 10, no. 1, 2018, Art. no. 107.
- [19] Y. Ma, S. Kang, L. Zhu, B. Xu, and T. Yao, "Roof of the world: Tibetan observation and research platform," *B Amer. Meteorol. Soc.*, vol. 89, no. 10, 2008, Art. no. 1487.
- [20] Z. Su, P. de Rosnay, J. Wen, L. Wang, and Y. Zeng, "Evaluation of ECMWF's soil moisture analyses using observations on the Tibetan plateau," *J. Geophys. Res., Atmospheres*, vol. 118, no. 11, pp. 5304–5318, Jun. 16, 2013.
- [21] K. Yang *et al.*, "A multiscale soil moisture and freeze–thaw monitoring network on the third pole," *Bull. Amer. Meteorological Soc.*, vol. 94, no. 12, pp. 1907–1916, 2013.
- [22] Y. Y. Liu *et al.*, "Developing an improved soil moisture dataset by blending passive and active microwave satellite-based retrievals," *Hydrol. Earth Syst. Sci.*, vol. 15, pp. 425–436, Jan./Feb. 2011. [Online]. Available: <https://ui.adsabs.harvard.edu/abs/2011HESS...15.425L>
- [23] T. N. Carlson, R. R. Gillies, and T. J. Schmugge, "An interpretation of methodologies for indirect measurement of soil water content," *Agricultural Forest Meteorol.*, vol. 77, no. 3, pp. 191–205, 1995.
- [24] I. Sandholt, K. Rasmussen, and J. Andersen, "A simple interpretation of the surface temperature/vegetation index space for assessment of surface moisture status," *Remote Sens. Environ.*, vol. 79, no. 2, pp. 213–224, 2002.
- [25] R. Tang, Z. Li, and B. Tang, "An application of the T-s-VI triangle method with enhanced edges determination for evapotranspiration estimation from MODIS data in and semi-arid regions: Implementation and validation," (in English), *Remote Sens. Environ.*, vol. 114, no. 3, pp. 540–551, Mar. 15, 2010. [Online]. Available: <Go to ISI>://WOS:000274820700009
- [26] N. S. Chauhan, S. Miller, and P. Ardanuy, "Spaceborne soil moisture estimation at high resolution: A microwave-optical/IR synergistic approach," (in English), *Int. J. Remote Sens.*, vol. 24, no. 22, pp. 4599–4622, Nov. 2003.
- [27] P. K. Srivastava, D. Han, M. A. Rico-Ramirez, D. Al-Shrafany, and T. Islam, "Data fusion techniques for improving soil moisture deficit using SMOS satellite and WRF-NOAH land surface model," *Water Res. Manage.*, vol. 27, no. 15, pp. 5069–5087, 2013.
- [28] D. F. Specht, "A general regression neural network," *IEEE Trans. Neural Netw.*, vol. 2, no. 6, pp. 568–576, Nov. 1991.
- [29] Y. Cui *et al.*, "A soil moisture spatial and temporal resolution improving algorithm based on multi-source remote sensing data and GRNN model," *Remote Sens.*, vol. 12, no. 3, 2020, Art. no. 455. [Online]. Available: <https://www.mdpi.com/2072-4292/12/3/455>
- [30] Y. Cui *et al.*, "A spatio-temporal continuous soil moisture dataset over the Tibet plateau from 2002 to 2015," *Sci. Data*, vol. 6, no. 1, Oct. 31, 2019, Art. no. 247.
- [31] C. Zeng, H. Shen, M. Zhong, L. Zhang, and P. Wu, "Reconstructing MODIS LST based on multitemporal classification and robust regression," *IEEE Geosci. Remote Sens. Lett.*, vol. 12, no. 3, pp. 512–516, Mar. 2015.
- [32] L. Jia, H. Shang, G. Hu, and M. Menenti, "Phenological response of vegetation to upstream river flow in the heihe rive basin by time series analysis of MODIS data," (in English), *Hydrol. Earth Syst. Sci.*, vol. 15, no. 3, pp. 1047–1064, 2011. [Online]. Available: <Go to ISI>://WOS:000288990400028
- [33] N. F. Liu *et al.*, "A statistics-based temporal filter algorithm to map spatiotemporally continuous shortwave albedo from MODIS data," *Hydrol. Earth Syst. Sci.*, vol. 17, no. 6, pp. 2121–2129, 2013.
- [34] L. Brocca *et al.*, "Improving runoff prediction through the assimilation of the ASCAT soil moisture product," (in English), *Hydrol. Earth Syst. Sci.*, vol. 14, no. 10, pp. 1881–1893, 2010. [Online]. Available: <Go to ISI>://WOS:000283667500007
- [35] Y. Chen *et al.*, "Evaluation of SMAP, SMOS, and AMSR2 soil moisture retrievals against observations from two networks on the Tibetan plateau," *JGR Atmos.*, vol. 122, no. 11, pp. 5780–5792, 2017.



Yaokui Cui received the B.S. degree in remote sensing science and technology from School of Remote Sensing and Information Engineering, Wuhan University, Wuhan, China, in 2008, the M.S. degree in photogrammetry and remote sensing from School of Earth and Space Science, Peking University, Beijing, China, in 2011, and the Ph.D. degree in Science from Institute of Remote Sensing and Digital Earth, Chinese Academy of Sciences, Beijing, China, in 2015.

He was a Postdoctoral Researcher with the Department of Hydraulic Engineering, Tsinghua University, Beijing, China. He is currently with the Institute of Remote Sensing and GIS, School of Earth and Space Sciences, Peking University. His current research interests focus on remote sensing evapotranspiration, soil moisture, and remote sensing big data. He has authored or coauthored more than 40 papers. He has also been the PI of more than four National Natural Funds and other research projects.



Chao Zeng received the B.S. degree in resources-environment and urban-rural planning management, the M.S. degree in surveying and mapping engineering, and the Ph.D. degree in photogrammetry and remote sensing from Wuhan University, Wuhan, China, in 2009, 2011, and 2014, respectively.

He was a Postdoctoral Researcher with the Department of Hydraulic Engineering, Tsinghua University, Beijing, China. He is currently with the School of Resources and Environmental Science, Wuhan University. His current research interests focus on remote sensing image processing and hydrological remote sensing applications.



Xi Chen received the Ph.D. degree in faculty of geographical science from Beijing Normal University, Beijing, China, in 2017.

Since 2017, he has been a Postdoctoral Researcher with the School of Earth and Space Sciences, Peking University, Beijing, China. He is currently an Assistant Research Fellow with the Aerospace Information Research Institute, Chinese Academy of Science, Beijing, China. His current research interests include the remote sensing big data of water cycle, the information extracting, fusing and application of land surface water, and underwater multisource data.



Wenjie Fan received the Ph.D. degree in physical geography from the College of Urban and Environmental Sciences, Peking University (PKU), Beijing, China, in 2000.

She completed the Post doctorate Research from the Institute of Remote Sensing and GIS (IRSGIS), PKU, in 2002. She is currently a Professor with the IRSGIS, PKU. She has continued to work on and manage research projects on vegetation remote sensing, scale effects of remote sensing, hyperspectral remote sensing, and application of remote sensing in ecology and environment management for 20 years. She has authored or coauthored more than 90 papers (more than 40 papers indexed by SCI). She has also been the PI of more than seven National Natural Funds and other research projects.



Haijiang Liu received the Ph.D. degree in cartography and geographical information system from Institute of Geographic Sciences and Natural Resources Research, Chinese Academy of Sciences, Beijing, China, in 2008. He is currently a Professorate Senior Engineer with the China National Environmental Monitoring Center, Beijing, China. His current research interests focus on ecosystem evaluation and ecological protection.



Yuan Liu received the M.S. degree in photogrammetry and remote sensing from Peking University, Beijing, China, in 2013.

Her research interests include vegetation remote sensing, re-collision probability, FAPAR retrieval, and other models of Quantitative Remote Sensing.



Wentao Xiong received the B.Eng. degree in geological engineering, in 2011 from Hebei GEO University, Shijiazhuang, China, the M.S. degree in petroleum geology, in 2014 from Peking University, Beijing, China, where he is currently working toward the Ph.D. degree in remote sensing.

Since 2014, he has been an Engineer with the School of Earth and Space Sciences, Peking University.



Cong Sun was born in Shandong, China, in 1985. He received the M.S. degree in soil and water conservation from the University of Chinese Academy of Sciences, Beijing, China, in 2010.

He is currently a Senior Engineer with the China National Environmental Monitoring Centre. His research interests are evaluation of ecological quality, ecological compensation mechanism, environmental monitoring, and evaluation.



Zengliang Luo received the Ph.D. degree in hydrology and water resources from Zhengzhou University, Zhengzhou, China, in 2019.

He is currently with the Peking University as a Postdoctoral Researcher. His research interests include distributed hydrological modeling, remote sensing hydrology, statistical hydrology, and water ecology experiment